2008

Fundamental Measure Density Functional Theory Studies on the Freezing of Binary Hard-Sphere and Lennard-Jones Mixtures

Vadim B. Warshavsky
Iowa State University

Xueyu Song
Iowa State University, xsong@iastate.edu

Fundamental Measure Density Functional Theory Studies on the Freezing of Binary Hard-Sphere and Lennard-Jones Mixtures

Abstract
Free energies and correlation functions of liquid and solid hard-sphere (HS) mixtures are calculated using the fundamental measure density functional theory. Using the thermodynamicperturbation theory the free energies of solid and liquid Lennard-Jones (LJ) mixtures are obtained from correlation functions of HS systems within a single theoretical approach. The resulting azeotrope- and spindle-type solid-liquidphase diagrams of HS and LJ binary mixtures are in good agreement with the corresponding ones from computer simulations.

Disciplines
Chemistry

Comments
The following article appeared in *Journal of Chemical Physics* 129 (2008): 034506, and may be found at doi:10.1063/1.2953329.

Fundamental measure density functional theory studies on the freezing of binary hard-sphere and Lennard-Jones mixtures

Vadim B. Warshavsky and Xueyu Song

Citation: The Journal of Chemical Physics **129**, 034506 (2008); doi: 10.1063/1.2953329
View online: http://dx.doi.org/10.1063/1.2953329
View Table of Contents: http://scitation.aip.org/content/aip/journal/jcp/129/3?ver=pdfcov
Published by the AIP Publishing

Fundamental measure density functional theory studies on the freezing of binary hard-sphere and Lennard-Jones mixtures

Vadim B. Warshavsky and Xueyu Song[a)]
Ames Laboratory and Department of Chemistry, Iowa State University, Ames, Iowa 50011, USA

(Received 7 May 2008; accepted 11 June 2008; published online 18 July 2008)

Free energies and correlation functions of liquid and solid hard-sphere (HS) mixtures are calculated using the fundamental measure density functional theory. Using the thermodynamic perturbation theory the free energies of solid and liquid Lennard-Jones (LJ) mixtures are obtained from correlation functions of HS systems within a single theoretical approach. The resulting azeotrope- and spindle-type solid-liquid phase diagrams of HS and LJ binary mixtures are in good agreement with the corresponding ones from computer simulations. © *2008 American Institute of Physics*. [DOI: 10.1063/1.2953329]

I. INTRODUCTION

Density functional theory (DFT) became a practical theoretical tool for the calculation of thermodynamic properties of binary hard-sphere (HS) mixtures. Using various approximate functionals, phase diagrams were calculated for substitutionally disordered fcc HS solid solutions coexisting with binary HS liquid mixtures.[1–4] The thermodynamic perturbation theory is a useful method to go beyond the HS systems to obtain thermodynamic properties of realistic systems. In the framework of the successful Weeks, Chandler, and Andersen (WCA) (Refs. 5 and 6) perturbation theory, the free energy is separated into two parts: One of them is the free energy of the reference system whereas the second one is the perturbation contribution, which can be obtained from the perturbation potential and the correlation functions of the reference system. The HS systems are often used as reference systems; hence, HS free energies and correlation functions are the essential inputs to the perturbation theory. In our previous study[7] we applied the WCA perturbation theory to calculate the free energies of one-component liquid and solid phases within a single theoretical framework. To this end the fundamental measure (FM) DFT (Refs. 8–10) was employed for the calculations of free energies and correlation functions in HS liquid and solid phases. Such information of the HS systems was used in the WCA perturbation theory to calculate the free energies of the Lennard-Jones (LJ) solid and liquid systems. Using the double-tangent Maxwell construction method we were able to calculate the solid-liquid coexistence for the single-component LJ system. The obtained results are in good agreement with the results from simulations. In the present report we extend that method to the binary mixture case to study solid-liquid phase equilibria of LJ mixtures.

We note that the WCA perturbation theory for single-component systems has already been generalized to the case of mixtures and has been applied to the LJ binary *liquid* mixtures.[11] In that work the results for free energies[12] and the theory for correlation functions[13,14] of the HS liquids were used for the liquid phase. Strategies for the separation of the pair potentials within the perturbation theory for liquid alloys were discussed in Ref. 15. The application of the perturbation theory to high-temperature mixture systems with Morse potentials was also performed.[16] It should be noted that applications of the perturbation theory to solid mixtures have not been studied yet due to the absence of accurate information of the HS solid mixture correlation functions. Recently we have developed an approach to calculate the correlation functions of HS solid mixtures.[17] Our approach is motivated by the method for the correlation functions of single-component HS solids[18] and is accurate for HS solid mixtures with moderate HS diameter asymmetry, as demonstrated by comparing the results from computer simulations.[17]

In the present work we use the free energies and the correlation functions of the HS solid mixtures obtained from FM DFT with the WCA perturbation theory to calculate the free energies of LJ solid mixtures. Integral equation method, which is also based on FM DFT, is employed to compute the correlation functions of HS liquid binary mixtures;[19] the results are used to compute the free energies of LJ liquid mixtures. Hence the LJ solid-liquid phase diagrams can be obtained via the double-tangent Maxwell construction. The fact that the solid and liquid free energies are calculated on the same theoretical footing may lead to more accurate results for phase equilibria.

Previously, solid-liquid phase diagrams of the binary LJ mixtures were obtained from experimental measurements,[20,21] cell theory,[22] and computer simulations.[23] To our knowledge, the present work is the first perturbation theory calculation of solid-liquid equilibria for binary LJ mixtures, and the methodology developed can be readily used for systems with various realistic potentials.

The rest of the paper is organized as follows. In Sec. II we summarize the perturbation theory of mixtures and the methods to calculate the free energies and the correlation functions of HS liquid and solid mixtures. In Sec. III we present the phase diagrams for HS and LJ binary mixtures,

a)Electronic mail: xsong@iastate.edu.

which are compared with the ones from computer simulations. Some concluding remarks are given in Sec. IV.

II. THEORY

A. The perturbation theory for the mixture free energy

For completeness and notational consistency we summarize the salient features for the calculation of free energies of liquid and solid binary mixtures using the thermodynamic perturbation theory.

Let $\psi_{ij}(r)$ be the interaction potential between a pair of particles of i and j species and r the distance between the particles. In the framework of the perturbation theory, $\psi_{ij}(r)$ is split into two parts,

$$\psi_{ij}(r) = \psi_{ij}^{(\mathrm{ref})}(r) + \psi_{ij}^{(\mathrm{pert})}(r), \tag{1}$$

where $\psi_{ij}^{(\mathrm{ref})}(r)$ is a short-ranged strong repulsive pair potential of the reference system and $\psi_{ij}^{(\mathrm{pert})}(r)$ is a weak attractive perturbation,

$$\psi_{ij}^{(\mathrm{ref})}(r) = \begin{cases} \psi_{ij}(r) - B_{ij}(r), & r \le \lambda_{ij} \\ 0, & r > \lambda_{ij}, \end{cases} \tag{2}$$

$$\psi_{ij}^{(\mathrm{pert})}(r) = \begin{cases} B_{ij}(r), & r \le \lambda_{ij} \\ \psi_{ij}(r), & r > \lambda_{ij}. \end{cases} \tag{3}$$

For normal liquid densities the separation parameters for the pair potentials λ_{ij} are chosen to be equal to r_{ij}^* [location of the potential $\psi_{ij}(r)$ minimum] and $B_{ij}(r) = \psi_{ij}(\lambda_{ij})$. For higher liquid densities near the freezing point, and also for solids,[24]

$$\lambda_{ij} = \min(r_{ij}^*, a_c) \tag{4}$$

and

$$B_{ij}(r) = \psi_{ij}(\lambda_{ij}) + (r - \lambda_{ij})\psi_{ij}'(\lambda_{ij}), \tag{5}$$

where a_c is the nearest-neighbor distance in the crystal (for fcc lattice $a_c = 2^{1/6}/\rho^{1/3}$; ρ is the total density of the system).

The next step in the perturbation theory formalism is a mapping from the reference system with potential $\psi_{ij}^{(\mathrm{ref})}(r)$ to a system of additive HSs with the interaction potential given by

$$\psi_{ij}^{(\mathrm{HS})}(r) = \begin{cases} +\infty, & r < d_{ij}(T) \\ 0, & r \ge d_{ij}(T). \end{cases} \tag{6}$$

All the temperature-dependent HS diameters $\{d_{ij}(T)\}$ can be found as a solution of the equations

$$I_{ij} = \int d\vec{r}(e^{-\beta\psi_{ij}^{(\mathrm{ref})}(r)} - e^{-\beta\psi_{ij}^{(\mathrm{HS})}(r)})y_{ij}(r) = 0, \tag{7}$$

where $y_{ij}(r)$ are the cavity functions, $\beta = 1/k_B T$, k_B is the Boltzmann constant, and T is the temperature. It should be noted that the additive condition of the HSs,

$$d_{12} = d_{21} = (d_{11} + d_{22})/2, \tag{8}$$

may not be satisfied as a result of the solution of Eq. (7). In this case the equations obtained from the conditions $I_{11} = I_{22} = 0$ [Eq. (7)] are solved to give the HS diameters d_{11} and d_{22}, whereas d_{12} is found from the condition in Eq. (8). The condition $I_{12} = 0$ from Eq. (7) can be fulfilled by adjusting the parameter λ_{12} for a given d_{12}.[15]

Finally the Helmholtz free energy for a binary mixture F can be written as

$$F = F_{\mathrm{HS}} + \frac{N\rho}{2}\sum_{i,j=1}^{2} x_i x_j \int d\vec{r} g_{ij}^{(\mathrm{HS})}(r)\psi_{ij}^{(\mathrm{pert})}(r). \tag{9}$$

In the right-hand side (rhs) of the equation the first contribution is the free energy of a HS system F_{HS} and the second one is the perturbation term and $g_{ij}^{(\mathrm{HS})}(r)s$ are the HS correlation functions.

For practical implementations, the conditions in Eq. (7) may be accurately approximated using the following relations:[11,13]

$$d_{ij} = d_{ij}^{(B)}\left(1 + \frac{\sigma_{ij}^{(1)}}{2\sigma_{ij}^{(0)}}\delta_{ij}\right), \tag{10}$$

where $d_{ij}^{(B)}s$ are the Barker–Henderson diameters,[25]

$$d_{ij}^{(B)} = \int_0^{\lambda_{ij}} (1 - e^{-\beta\psi_{ij}^{(\mathrm{ref})}(r)})dr, \tag{11}$$

and small parameters $\delta_{ij}s$ are given by

$$\delta_{ij} = \int_0^{\lambda_{ij}} \left(\frac{r}{d_{ij}^{(B)}} - 1\right)^2 \frac{d}{dr} e^{-\beta\psi_{ij}^{(\mathrm{ref})}(r)} dr. \tag{12}$$

The quantities $\sigma_{ij}^{(0)}$ and $\sigma_{ij}^{(1)}$ in the rhs of Eq. (10) depend on the diameters d_{ij},

$$\sigma_{ij}^{(0)} = y_{ij}(d_{ij}), \quad \sigma_{ij}^{(1)} = 2\sigma_{ij}^{(0)} + r\frac{dy_{ij}}{dr}\bigg|_{r=d_{ij}}. \tag{13}$$

Thus, a set of parameters, λ_{11}, λ_{22}, $d_{11}^{(B)}$, $d_{22}^{(B)}$, and δ_{11}, δ_{22} can be found from Eqs. (4), (11), and (12). If we know the dependence of $g_{ij}(r)$ on $\{d_{ij}\}$ (see Sec. II C and II D) then the HS diameters d_{11} and d_{22} can be obtained by one step iterative solutions of Eq. (10), with initial guesses $d_{11}^{(B)}$ and $d_{22}^{(B)}$. As we mentioned before the collision diameter d_{12} is found from Eq. (8), whereas λ_{12} is obtained from the solutions of Eq. (7) [or Eq. (10)], with $i \neq j$ [to ensure that the potential $\phi_{12}^{(\mathrm{ref})}(r)$ is pure repulsive, the condition $\lambda_{12} \le r_{12}^*$ should be satisfied].

B. The FM DFT and free energies of HS mixture

In this section we outline the method to calculate the free energies of HS liquid and solid mixtures F_{HS} using the FM DFT. Consider a mixture of HSs with diameters d_{11} and d_{22} $(d_{11} < d_{22})$ and bulk number densities ρ_1 and ρ_2. This mixture can be characterized by three parameters: The total packing fraction

$$\eta = \frac{\pi}{6}\rho_1 d_{11}^3 + \frac{\pi}{6}\rho_2 d_{22}^3, \tag{14}$$

the molar fraction of the larger sphere $x = \rho_2/(\rho_1 + \rho_2)$, and the ratio of HS diameters $\delta = d_{11}/d_{22}$.

In the framework of the density functional approach, the Helmholtz free energy of HS binary mixtures F_{HS} is expressed as a function of the density profiles of each component $\{\rho_i(\vec{r})\}$,[26]

$$F_{\mathrm{HS}}[\rho_1(\vec{r}),\rho_2(\vec{r})] = k_BT\sum_{i=1}^{2}\int d\vec{r}\rho_i(\vec{r})\{\log(\rho_i(\vec{r})\Lambda_i^3)-1\} + F^{(\mathrm{ex})}[\rho_1(\vec{r}),\rho_2(\vec{r})], \quad (15)$$

where the first term is the ideal gas contribution, $F^{(\mathrm{ex})}$ is the excess free energy functional, and Λ_1 and Λ_2 are the thermal de Broglie wavelengths. Various approximations to $F^{(\mathrm{ex})}$ are available for the binary mixture systems.[1–4] It is known that the FM density functional is the most accurate one to describe the single-component HS solid crystal.[9,10] In the present report we use the FM DFT to study HS binary mixtures, and our results indicate that this DFT is also accurate for the thermodynamic properties of HS binary mixtures if $\delta > 0.9$.

The excess part of the FM free energy density functional is given by[9,10]

$$F^{(\mathrm{ex})} = k_BT\int d\vec{r}\Phi[n_\alpha(\vec{r})], \quad (16)$$

where

$$\Phi = -n_0\ln(1-n_3) + \frac{n_1n_2-\vec{n}_{v_1}\vec{n}_{v_2}}{(1-n_3)} + \frac{1}{8\pi n_3^2}\left(\frac{n_3}{(1-n_3)^2}+\ln(1-n_3)\right)\{\vec{n}_{v_2}\hat{n}\vec{n}_{v_2}-n_2\vec{n}_{v_2}^2-tr(\hat{n}^3) + n_2tr(\hat{n}^2)\}. \quad (17)$$

The scalars n_0, n_1, n_2, n_3, vectors $\vec{n}_{v_1}$ $\vec{n}_{v_2}$, and tensor $\hat{n}_{ij}$ in the expression are the weighted densities obtained from the densities $\{\rho_i(\vec{r})\}$ by the following integral convolutions:

$$n_\alpha(\vec{r}) = \sum_{i=1}^{2}\int d\vec{r}'\rho_i(\vec{r}')\omega_i^{(\alpha)}(\vec{r}-\vec{r}'), \quad (18)$$

with the corresponding weight functions $\omega_i^{(\alpha)}(r)$,

$$\omega_i^{(2)}(r) = \delta\left(\frac{d_{ii}}{2}-r\right), \quad \omega_i^{(3)}(r) = \Theta\left(\frac{d_{ii}}{2}-r\right),$$

$$\omega_i^{(0)}(r) = \frac{1}{\pi d_{ii}^2}\omega_i^{(2)}(r), \quad \omega_i^{(1)}(r) = \frac{1}{2\pi d_{ii}}\omega_i^{(2)}(r),$$

$$\vec{\omega}_i^{(v_2)}(\vec{r}) = \frac{\vec{r}}{r}\delta\left(\frac{d_{ii}}{2}-r\right), \quad \vec{\omega}_i^{(v_1)}(\vec{r}) = \frac{1}{2\pi d_{ii}}\vec{\omega}_i^{(v_2)}(\vec{r}),$$

$$\hat{\omega}_i^{(jk)}(\vec{r}) = \frac{r_jr_k}{r^2}\delta\left(\frac{d_{ii}}{2}-r\right). \quad (19)$$

In the above expressions $\delta(r)$ is the Dirac delta function, $\Theta(r)$ is the Heaviside step function, and $\{r_k\}$ are the components of vector $\vec{r}$.

In a solid mixture the local one-body densities are not uniform. They can be parametrized as a sum of Gaussian density distributions centered at the crystal lattice sites. For a substitutionally disordered fcc solid solution, a given site is considered to be occupied by the particles of both components, with the probability equal to the corresponding concentration. Thus,

$$\rho_i(\vec{r}) = x_i\left(\frac{\alpha_i}{\pi}\right)^{3/2}\sum_{\vec{R}_k}e^{-\alpha_i(\vec{r}-\vec{R}_k)^2} \quad (i=1,2). \quad (20)$$

In the above expression α_1 and α_2 are the parameters of the Gaussian distributions; the sum runs over all the fcc lattice sites $\{\vec{R}_k\}$. Using Eq. (20) all the weighted densities $\{n_\alpha\}$ [Eq. (18)] can be calculated from explicit analytical expressions, and the volume integration in Eqs. (15) and (16) can be performed on a small volume simplex reflecting the symmetry of the crystal (for details of the calculations for the single-component case, see Refs. 7, 27, and 28).

In the implementations below we will write the free energy functional in the form

$$F_{\mathrm{HS}}[\rho_1(\vec{r}),\rho_2(\vec{r})] = F^{(i)}+F^{(e)}, \quad (21)$$

where $F^{(i)} = k_BT\Sigma_{i=1}^{2}\int d\vec{r}\rho_i(\vec{r})\{\log(\rho_i\Lambda_i^3)-1\}$ and

$$F^{(e)} = k_BT\sum_{i=1}^{2}\int d\vec{r}\rho_i(\vec{r})\log(\rho_i(\vec{r})/\rho_i) + k_BT\int d\vec{r}\Phi[n_\alpha(\vec{r})]. \quad (22)$$

Due to the normalization conditions $\rho_i = (1/V)\int d\vec{r}\rho_i(\vec{r})$ (V is the volume of the system), we have

$$F^{(i)} = k_BTV\sum_{i=1}^{2}\rho_i\{\log(\rho_i\Lambda_i^3)-1\}. \quad (23)$$

It is seen that the expression for $F^{(i)}$ is independent of α_1 and α_2, as well as of HS diameters d_{11} and d_{22}. Finally, for given parameters of a mixture η, x, and δ, minimization of the free energy functional with respect to α_1 and α_2 yields the equilibrium solid mixture free energy $F_{\mathrm{HS}}[\eta,x,\delta]$ and the Gaussian parameters α_1 and α_2 for the density profile.

For a binary liquid mixture the one-body densities of each component are uniform $\rho_i(\vec{r}) = \rho_i$ ($i=1,2$). Substituting this into Eqs. (16)–(19) the free energy functional of Eq. (15) in the homogeneous case reduces to the Boublik–Monsouri-Carnahan–Staling–Leland (BMCSL) formula[12,29] for the free energy of HS liquid mixtures, which is known to be accurate from comparisons with simulation results.[30]

C. The correlation functions of binary HS solid mixtures

In this section we briefly summarize the calculation of the correlation functions for HS solid binary mixtures $g_{ij}(r)$ (for more details see Ref. 17). An angle-averaged correlation function in a solid phase can be defined as

$$\tilde{g}_{ij}(r) = \frac{1}{4\pi V\rho_i\rho_j}\int d\vec{r}_1\int d\omega\rho_{ij}^{(2)}(\vec{r}_1,\vec{r}_1+\vec{r}), \quad (24)$$

where $\rho_{ij}^{(2)}(\vec{r}_1,\vec{r}_2)$ is the two particle distribution function and $d\omega$ is the differential solid angle element around $\vec{r}$. If we

assume that $\rho_{ij}^{(2)}(\vec{r}_1,\vec{r}_2)=\rho_j(\vec{r}_1)\rho_i(\vec{r}_2)$ (a mean-field approximation) then Eq. (24) gives

$$g_{ij}^{(0)}(r)=\sum_{k\geq 0} g_{k,ij}^{(0)}(r), \tag{25}$$

where

$$g_{k,ij}^{(0)}(r)=\frac{n_k}{4\rho\pi r R_k}\left(\frac{\alpha_i\alpha_j}{(\alpha_i+\alpha_j)\pi}\right)^{1/2} \times\{e^{-\alpha_i\alpha_j/(\alpha_i+\alpha_j)(r-R_k)^2}-e^{-\alpha_i\alpha_j/(\alpha_i+\alpha_j)(r+R_k)^2}\}. \tag{26}$$

Here k runs over the number of the successive lattice shells, and n_k and R_k are the coordination number and distance of the kth lattice shell.

To account for the short-ranged correlations between the particles that affect mostly the particles within the first coordination shell (the nearest neighbors), we can write the correlation functions $g_{ij}(r)$ as

$$g_{ij}(r)=g_{1,ij}(r)+\sum_{k\geq 2} g_{k,ij}^{(0)}(r). \tag{27}$$

To find $g_{1,ij}(r)$ in Eq. (27) we proposed the following parametrization:

$$g_{1,ij}(r)=A_{ij}\frac{e^{-\alpha'_{ij}/2(r-r_1)^2}}{r}, \quad r\geq d_{ij}, \tag{28}$$

with $g_{1,ij}(r)=0$ for $r<d_{ij}$. To find the seven parameters $\{A_{ij}\}$, $\{\alpha'_{ij}\}$, and r_1 of this parametrization, seven independent constraints are needed. Three of them are the conditions related to the contact values of the correlation functions $\{g_{ij}(d_{ij})\}$,

$$\frac{\beta P}{\rho}=1+\frac{2\pi}{3}\rho\sum_{i,j=1}^{2} x_i x_j d_{ij}^3 g_{ij}(d_{ij}), \tag{29}$$

$$\frac{\partial}{\partial\delta}\left(\frac{\beta F^{(e)}}{N}\right)\bigg|_{\eta,x}=\frac{2\pi\rho d_{22}x_1x_2}{(x_1\delta^3+x_2)}\sum_{i=1}^{2} x_i\{d_{1i}^2 g_{1i}(d_{1i}) -\delta^2 d_{2i}^2 g_{2i}(d_{2i})\}, \tag{30}$$

$$g_{12}(d_{12})=[g_{11}(d_{11})g_{22}(d_{22})]^{1/2}, \tag{31}$$

where P is pressure. The compressibility factor at the left-hand side of Eq. (29) can be calculated from $\frac{\beta P}{\rho}=1+\eta(\partial/\partial\eta)\left(\frac{\beta F^{(e)}}{N}\right)|_{x,\delta}$.

The next group of conditions are the normalization of the functions $g_{1,ij}(r)$ to the nearest-neighbor number,

$$\rho\int d\vec{r}\,\tilde{g}_{1,ij}(r)=n_1 \quad (i,j=1,2). \tag{32}$$

The final condition is an approximation for the mean location of the nearest neighbors $\langle r\rangle$,

$$\sum_{i,j=1}^{2} x_i x_j\int d\vec{r} r g_{1,ij}(r)=\sum_{i,j=1}^{2} x_i x_j\int d\vec{r} r g_{1,ij}^{(0)}(r)=\frac{n_1}{\rho}\langle r\rangle. \tag{33}$$

The FM density functional is used to compute α_1, α_2, $\beta P/\rho$, and $(\partial/\partial\delta)\left(\frac{\beta F^{(e)}}{N}\right)$. The solution to the set of Eqs. (28)–(33) gives all the needed parameters $\{A_{ij}\}$, $\{\alpha'_{ij}\}$, and r_1 of the first peak parameterization [Eq. (28)] and, thus, the correlation functions in Eq. (27).

The correlation functions become more accurate for moderately asymmetric solid mixtures, i.e., for ones with the diameter ratio δ being higher than 0.90,[17] which are in the range of δ used in the perturbation calculations in this report.

D. The correlation functions of HS liquid binary mixtures

For completeness we also outline the calculation of the correlation functions $g_{ij}(r)$ for the HS liquid binary mixture using the FM density functional.[19] Consider a HS liquid binary mixture with a test particle of j type fixed at the origin. The grand canonical density functional of this system is

$$\Omega_{\rm HS}[\rho_{1j}(\vec{r}),\rho_{2j}(\vec{r})]=F_{\rm HS}[\rho_{1j}(\vec{r}),\rho_{2j}(\vec{r})] -\sum_{i=1}^{2}\int d\vec{r}\rho_{ij}(\vec{r})\{\mu_i-\psi_{ij}^{(\rm HS)}(\vec{r})\}, \tag{34}$$

where $\rho_{ij}(\vec{r})$ is the density profile of i particles in the external field of the fixed particle j, μ_i is the chemical potential of i-type particles (it can be found from BMCSL equation of state), and $\psi_{ij}^{(\rm HS)}(\vec{r})$ is the external potential of HS interaction [Eq. (6)]. The variational principle,[26]

$$\frac{\delta\Omega_{\rm HS}[\rho_{1j}(\vec{r}),\rho_{2j}(\vec{r})]}{\delta\rho_{1j}(\vec{r})}\bigg|_{\vec{\mu},T}=0, \quad \frac{\delta\Omega_{\rm HS}[\rho_{1j}(\vec{r}),\rho_{2j}(\vec{r})]}{\delta\rho_{2j}(\vec{r})}\bigg|_{\vec{\mu},T}=0, \tag{35}$$

where $\vec{\mu}=(\mu_1,\mu_2)$ yields the equilibrium density profiles $\rho_{1j}(\vec{r})$ and $\rho_{2j}(\vec{r})$.

Since in an open system the normalization $\rho_i=(1/V)\int d\vec{r}\rho_{ij}(\vec{r})$ is not valid anymore (the differences $\int d\vec{r}[\rho_{ij}(\vec{r})/\rho_i-1]$, which are so-called Kirkwood–Buffs integrals, can be found from the thermodynamic properties of mixtures[31]), in this section we use the HS free energy functional in the form of Eq. (15) rather than Eqs. (21)–(23).

Substituting Eqs. (15) and (34) into Eq. (35), we have a set of equations for the density profiles of the particles of one and two types in the external field of the fixed particle of j-type $(j=1,2)$

$$\rho_{1j}(r)=\rho_1\exp\left\{-\frac{\delta\beta F^{(\rm ex)}[\rho_{1j}(\vec{r}),\rho_{2j}(\vec{r})]}{\delta\rho_{1j}(\vec{r})} +\beta\mu_1^{(\rm ex)}-\beta\psi_{1j}^{(\rm HS)}(r)\right\}, \tag{36}$$

$$\rho_{2j}(r)=\rho_2\exp\left\{-\frac{\delta\beta F^{(\rm ex)}[\rho_{1j}(\vec{r}),\rho_{2j}(\vec{r})]}{\delta\rho_{2j}(\vec{r})} +\beta\mu_2^{(\rm ex)}-\beta\psi_{2j}^{(\rm HS)}(r)\right\}, \tag{37}$$

where $\mu_i^{(\rm ex)}=\mu_i-k_BT\log(\rho_i\Lambda_i^3)$ $(i=1,2)$ is the excess part of chemical potential. The functional derivatives in the above

equations can be written using Eqs. (16) and (18) as

$$\frac{\delta\beta F^{(\mathrm{ex})}[\rho_{1j}(\vec{r}),\rho_{2j}(\vec{r})]}{\delta\rho_{ij}(\vec{r})} = \int d\vec{r}' \sum_{\alpha} \frac{\partial\Phi}{\partial n_\alpha}\omega_i^{(\alpha)}(\vec{r}-\vec{r}'). \quad (38)$$

If a density distribution has a radial symmetry as it has in an isotropic liquid, then the three-dimensional integrals in Eq. (18) to find all $n^{(\alpha)}$ and in Eq. (38) to find $\delta\beta F^{(\mathrm{ex})}/\delta\rho_{ij}$ can be reduced to one-dimensional integrals. As a result, the set of Eqs. (36) and (37) can be solved by Picard iterations, with the bulk densities ρ_i as initial guesses for $\rho_{ij}(r)$. To overcome difficulties with the iteration convergence, a mixing scheme is used. For more details of the calculations in a single-component case, see Ref. 7. Finally the correlation function can be found from the following relation:[32]

$$g_{ij}(r) = \rho_{ij}(r)/\rho_i. \quad (39)$$

The condition $g_{12}(r)=g_{21}(r)$ provides a way to check if the calculations are correct.

III. RESULTS

Using the methods outlined in the previous sections, we should be able to calculate Helmholtz free energies per particle $F(x,\rho,T)/N$ for the binary solid and liquid mixtures. To calculate Gibbs free energies per particle $G(x,P,T)/N$, we have

$$\frac{G(x,P,T)}{N} = \frac{F(x,\rho,T)}{N} + \frac{P}{\rho}. \quad (40)$$

The dependence of ρ on the variables x, P, and T can be found from the condition

$$P = \rho^2 \frac{\partial}{\partial\rho}\left(\frac{F(x,\rho,T)}{N}\right)_{x,T}. \quad (41)$$

To solve Eq. (41) we introduce the function $\tilde{g}(x,\rho,P,T)=F(x,\rho,T)/N+P/\rho$. The difference between $\tilde{g}$ and G/N is that $\tilde{g}$ has the density ρ as an argument, which is independent of x, P, and T. Numerical minimization of the function $\tilde{g}$ with respect to ρ yields the density ρ, which satisfies the condition in Eq. (41), i.e., $\tilde{g}$ at the minimum to be equal to G/N.

For a given pressure P and temperature T, we plot the dependence of the Gibbs free energy G/N on x both for solid and liquid phases on the same graph. For fixed P and T, the liquid and solid phases coexist when their chemical potentials of each species are equal, i.e.,

$$\mu_1^{(l)} = \mu_1^{(s)}, \quad \mu_2^{(l)} = \mu_2^{(s)}. \quad (42)$$

These conditions are satisfied at concentrations x_l and x_s, which are the points of a common tangent to the liquid and solid G/N vs x curves. As a matter of fact, at these points the two relations $\mu_2^{(l)}-\mu_1^{(l)}=\mu_2^{(s)}-\mu_1^{(s)}$ and $\mu_1^{(l)}=\mu_1^{(s)}$ are satisfied using

$$\mu_2-\mu_1 = \frac{\partial}{\partial x}\left(\frac{G}{N}\right), \quad \mu_1 = \frac{G}{N} - x\frac{\partial}{\partial x}\left(\frac{G}{N}\right), \quad (43)$$

which leads to Eq. (42). Varying temperature T at fixed pressure P and repeating the above procedure, a temperature-concentration (T vs x) phase diagram can be constructed.[4]

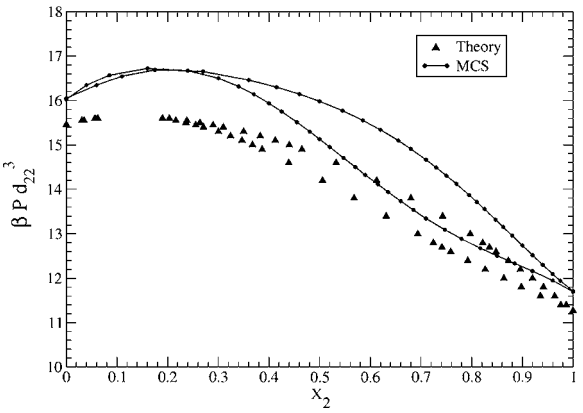

FIG. 1. An azeotrope-type pressure vs composition (P^*-x) phase diagram for binary HS mixture at the diameter ratio δ=0.90. The result of the theory is compared with the one from simulations (Ref. 33).

A. The HS mixtures

To test the present version of FM DFT we calculated the phase diagrams for HS solid-liquid mixtures. We note that in the HS systems it is convenient to measure the free energy per particle, F/N, relative to the value $k_BT\Sigma_{i=1}^2 x_i \log\left(\frac{\Lambda_i^3}{d_{ii}^3}\right)$ because it has no influence on the result of the double-tangent construction. As a result, the Helmholtz free energy F/N, the Gibbs free energy G/N, and the pressure P have only a simple linear dependence on T; therefore, it is appropriate to work with dimensionless values $\beta F(x,\eta,\delta)/N$, $\beta G(x,P^*,\delta)/N$, and $P^*=\beta P d_{22}^3$.

For a given value of HS diameters ratio δ and pressure P^*, we plot the dependence of solid and liquid Gibbs free energy per particle $\beta G/N$ on x on the same graph. Again the pressure-composition (P^*-x) phase diagrams are constructed using the common-tangent method. Figures 1 and 2 show the resulting phase diagrams for the values of diameter ratio δ=0.90,0.95. For comparison the Monte Carlo simulation (MCS) data[33] are also shown. It is seen that for δ=0.90 (the azeotrope-type phase diagram) and δ=0.95 (the spindle-type phase diagram) the results are in good agreement with the ones from simulations.[33] As a matter of fact, the theory un-

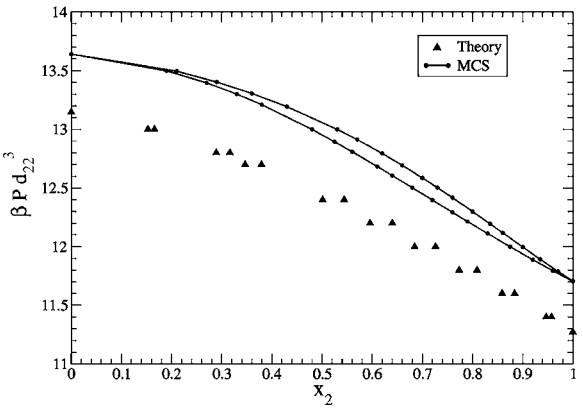

FIG. 2. A spindle-type pressure vs composition (P^*-x) phase diagram for binary HS mixture at the diameter ratio δ=0.95. The result of the theory is compared with the one from simulations (Ref. 33).

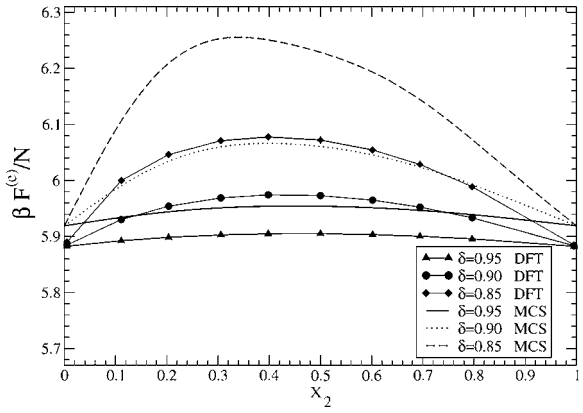

FIG. 3. Dependence of the Helmholtz free energy $\beta F^{(e)}/N$ of HS solid mixtures on composition x for HS diameter ratios $\delta=0.95$, 0.90, 0.85 and $\eta=0.545$. The results of the FM DFT are compared with the ones from simulations (Ref. 30).

derestimates the freezing pressures P_f^* compared to the ones from simulations. Thus, for the single-component HS system the equilibrium pressure P_f^* from the present version of FM DFT (Refs. 9 and 10) is 11.3 (to our knowledge this particular result was not published) and the P_f^* from the simulations[33,34] is 11.7. Thus, the difference between these two results is about 4%. For mixtures this difference is less than 5% for $\delta=0.95$ for any molar fraction x and it is less than 8% for $\delta=0.90$. The agreement between the theory and simulations will improve if the simulation data are plotted against a different scale to ensure the perfect agreement between the theory and simulations at $x=0$ and $x=1$, as presented in Ref. 4.

The solid packing fraction η_s along the coexistence lines is in the range of [0.535:0.543] for $\delta=0.90$ and of [0.535:0.537] for $\delta=0.95$ (the FM DFT result for a single-component case $\eta_s=0.535$ is close to the MCS one $\eta_s=0.545$).

In order to reduce the sources of errors for the perturbation theory, the treatment of the reference system should be very accurate. In Fig. 3 we show the dependence of HS free energy $\beta F^{(e)}/N$ on x for $\delta=0.95, 0.90, 0.85$ and $\eta=0.545$ and compare the results with the ones from simulations. For given η, x, and δ, the value of $\beta F^{(e)}/N$ from the DFT is lower than the corresponding ones from MCS.[30] The maximum difference between these two values are about 0.8% for $\delta=0.95$, 1.5% for $\delta=0.90$, and 2.9% for $\delta=0.85$. We also found that increasing the value of solid packing fraction η makes this difference larger (especially for $\delta=0.85$), while decreasing η makes the difference smaller. Thus, the FM DFT is accurate and well suitable for the perturbation theory calculations of solid mixture properties with moderate HS diameter asymmetry. We will see in the next section that the parameters of the reference HS systems are $\eta_s \leq 0.55$ and $\delta_s \geq 0.90$ along the solid-liquid LJ mixture coexistence (Table I). Within these parameter ranges, FM DFT provides accurate thermodynamic properties and can be used for the perturbation theory.

B. The LJ mixtures

In this section we applied the thermodynamic perturbation theory to calculate the solid-liquid phase diagrams for LJ binary mixtures with interparticle potential,

$$\psi_{ij}^{(\mathrm{LJ})}(r) = 4\epsilon_{ij}\left\{\left(\frac{\sigma_{ij}}{r}\right)^{12} - \left(\frac{\sigma_{ij}}{r}\right)^{6}\right\} \quad (i,j=1,2), \tag{44}$$

where ϵ_{ij} is the LJ attractive well depth and σ_{ij} is the LJ diameter. The Lorentz–Berthelot mixing rules $\sigma_{12}=(\sigma_{11}+\sigma_{22})/2$ and $\epsilon_{12}=\sqrt{\epsilon_{11}\epsilon_{22}}$ define the cross-species interaction parameter $(\sigma_{12}, \epsilon_{12})$. We will use argon-methane $ArCH_4$ and argon-krypton ArKr as model LJ mixtures to show that our theory is able to reproduce the azeotrope- and spindle-type solid-liquid phase diagrams of these systems. The well depth ϵ_{ii} and diameter σ_{ii} for Ar, Kr, and CH_4 are given in Ref. 35.

Figure 4 shows the dependence of $ArCH_4$ liquid and solid Gibbs free energies per particle G/N on the composition x_{CH_4} at pressure $P=1$ atm and different temperatures

TABLE I. The parameters at the coexistence of the ArKr and $ArCH_4$ mixture systems for various temperatures T: Liquid and solid compositions x_l and x_s and number densities ρ_l and ρ_s. The parameters of reference liquid and solid HS systems at coexistence: The packing fractions η_l and η_s and the diameter ratios δ_l and δ_s.

T (K)	x_l	x_s	ρ_l (Å^{-3})	ρ_s (Å^{-3})	η_l	η_s	δ_l	δ_s
$ArCH_4$								
100	0.0789	0.0198	0.0218	0.0255	0.47	0.54	0.91	0.95
95	0.1627	0.1036	0.0217	0.0252	0.48	0.55	0.91	0.94
95	0.5025	0.5813	0.0199	0.0220	0.50	0.55	0.90	0.92
100	0.6108	0.6995	0.0190	0.0211	0.49	0.55	0.90	0.91
105	0.7241	0.7979	0.0181	0.0203	0.48	0.55	0.90	0.90
110	0.8620	0.9161	0.0172	0.0193	0.48	0.55	0.90	0.90
ArKr								
105	0.0937	0.1233	0.0217	0.0249	0.46	0.53	0.92	0.95
110	0.2464	0.2907	0.0211	0.0240	0.47	0.53	0.92	0.94
115	0.3252	0.3744	0.0205	0.0235	0.46	0.53	0.92	0.94
120	0.4335	0.4877	0.0201	0.0229	0.46	0.53	0.92	0.93
125	0.5665	0.6157	0.0195	0.0223	0.46	0.53	0.92	0.93
130	0.7438	0.7782	0.0189	0.0217	0.46	0.54	0.92	0.92
135	0.9112	0.9309	0.0184	0.0211	0.46	0.54	0.92	0.93

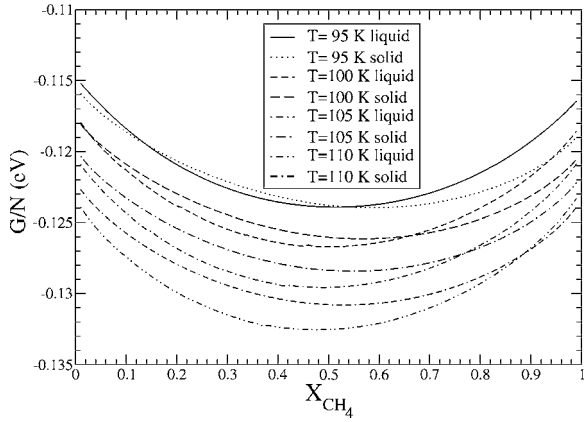

FIG. 4. Dependence of the liquid and solid Gibbs free energies per particle G/N (eV) on x_{CH_4} for the binary $ArCH_4$ system at fixed pressure $P=1$ atm and the temperatures $T=95$, 100, 105, and 110 K.

$T=95$, 100, 105, and 110 K. It is seen that for higher temperatures $T=105$ and 110 K, the $G^{(s)}/N$ and $G^{(l)}/N$ curves have one intersection point whereas for lower temperatures $T=95$ and 100 K there are two intersection points. Figure 5 shows the temperature-composition (T-x) phase diagram for the $ArCH_4$ mixture system, along with the simulation results.[23] The calculated azeotrope phase diagram is in reasonable agreement with the one from simulations. For example, for any given molar fraction x_{CH_4} the freezing temperature T_f from the perturbation calculation overestimates the corresponding simulation value by about 5%. We can conclude that the accuracy of the theory for $ArCH_4$ mixture is comparable to the ones for the pure components of Ar and CH_4.

In Table I, the parameters of $ArCH_4$ coexisting solid and liquid phases for some selected temperatures T are given. These parameters are the coexisting liquid and solid compositions x_l and x_s and number densities ρ_l and ρ_s. We also put in Table I the parameters of the corresponding reference HS systems at coexistence: Liquid and solid packing fractions η_l and η_s and the diameter ratios δ_l and δ_s. It is seen that the ranges of values for δ_l and δ_s are within [0.90:0.91] and [0.90:0.95], respectively.

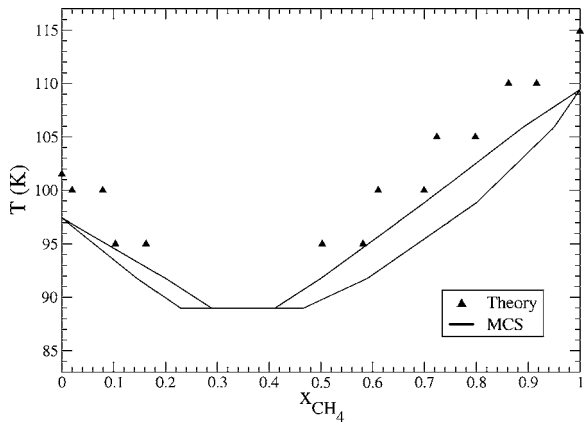

FIG. 5. Temperature-composition (T-x) liquid-solid phase diagram for the binary $ArCH_4$ system at $P=1$ atm. The result of the theory is compared with the one from simulations (Ref. 23).

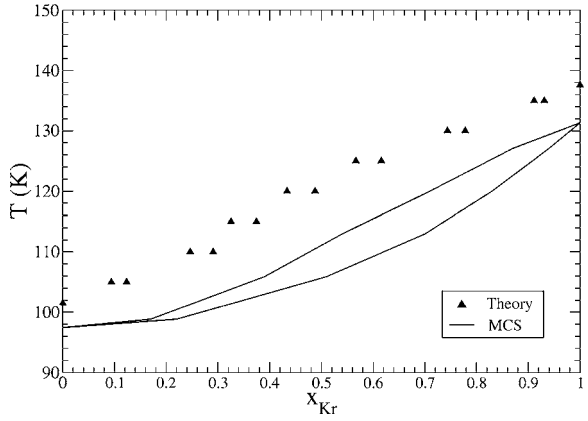

FIG. 6. Temperature-composition (T-x) liquid-solid phase diagram for the binary ArKr system at $P=1$ atm. The result of the theory is compared with the one from simulations (Ref. 23).

Figure 6 shows the temperature-composition (T-x) phase diagram for the ArKr system, along with the simulation results.[23] We obtain a spindle-type phase diagram, which again is in reasonable agreement with the simulation data. For single-component Ar and Kr the freezing temperatures T_f from the perturbation theory are about 5% higher than the ones from the simulations. For the ArKr mixtures with a given molar fraction x_{Kr}, the difference between the freezing temperature T_f from the theory and the simulations is less than 11%. Thus, for this mixture the theory provides the results that are a bit less accurate compared to ones for the pure components Ar and Kr.

In Table I we also provide the parameters of ArKr coexisting phases for some temperatures. It is seen that the HS diameter ratio δ_l is equal to 0.92 and δ_s is within the range of [0.92:0.95]. We notice that for ArKr mixture the values of δ_l and δ_s are somewhat higher than the ones for $ArCH_4$ mixture; however they still belong to the range δ, where azeotropic-type phase diagram of the pure HS mixture is transformed into the spindle-type one.

To conclude this subsection we note that for the binary systems with attractive intermolecular potentials, the analysis of diameter ratios δ of the reference HS systems is not enough to predict the type of the solid-liquid phase diagram. Some additional factors of the intermolecular attraction (such as the ratio $\epsilon_{11}/\epsilon_{22}$) are needed to be taken into consideration.

IV. CONCLUSIONS

In the present study we have developed a method to compute the free energies of the solid and liquid molecular mixtures within a single theoretical approach without inputs from simulations. Using the fundamental measure DFT free energies and correlation functions of the reference HS liquid and solid mixture systems can be obtained. With these inputs to the thermodynamic perturbation theory, the free energies of the solid and liquid LJ mixtures were calculated. The perturbation theory for solid mixtures becomes more accurate if the parameters of the reference HS mixture are in the range of $\delta \geq 0.90$ and $\eta \leq 0.55$. We note that these conditions are satisfied for all the considered molecular mixtures (see Table

I) in this report. The obtained azeotrope- and spindle-type phase diagrams are in reasonable agreement with the corresponding ones from computer simulations.[23,33]

We note that the parameters of the solid-liquid equilibria could be calculated using a combination of the thermodynamic perturbation theory and Gibbs–Duhem integration technique.[36] It is interesting to compare the results obtained using this method with the ones computed in the present study via Maxwell construction and also using the simulations.[23]

Our method can also be extended to study the solid-liquid phase equilibria of mixtures with molecules interacting via the angle-dependent potentials, such as LJ dumbbells[37] or Stockmayer molecules.[38,39] Applications of the method to metallic alloys with embedded-atom model potentials are also very promising.[40] Since within our approach the solid and liquid mixtures are treated using a single theoretical method it may be possible to apply this approach to investigate the interface between solid and liquid mixtures.[41]

Our method can be generalized to study solid-liquid phase equilibria in ternary mixtures because the involved theories, such as the perturbation theory, the FM DFT for HS free energies, and the approaches to calculate the correlation functions in HS solid and liquid mixtures can be straightforwardly generalized to such multicomponent mixtures.

ACKNOWLEDGMENTS

This research was sponsored by the Division of Materials Sciences and Engineering, Office of Basic Energy Sciences, U.S. Department of Energy, under Contract No. W-7405-ENG-82 with Iowa State University (V.B.W. and X.S.) and by PRF Grant No. 46451AC6 (X.S.).

[1] J. L. Barrat, M. Baus, and J. P. Hansen, J. Phys. C **20**, 1413 (1987).
[2] S. W. Rick and A. D. J. Haymet, J. Phys. Chem. **94**, 5212 (1990).
[3] X. C. Zeng and D. W. Oxtoby, J. Chem. Phys. **93**, 4357 (1990).
[4] A. R. Denton and N. W. Ashcroft, Phys. Rev. A **42**, 7312 (1990).
[5] J. D. Weeks, D. Chandler, and H. C. Andersen, J. Chem. Phys. **54**, 5237 (1971).
[6] D. Chandler, J. D. Weeks, and H. C. Andersen, Science **220**, 786 (1983).
[7] V. B. Warshavsky and X. Song, Phys. Rev. E **69**, 061113 (2004).
[8] Y. Rosenfeld, Phys. Rev. Lett. **63**, 980 (1989).
[9] R. Roth, R. Evans, A. Lang, and G. Kahl, J. Phys.: Condens. Matter **14**, 12063 (2002).
[10] P. Tarazona, Physica A **306**, 243 (2002).
[11] L. L. Lee and D. Levesque, Mol. Phys. **26**, 1351 (1973).
[12] G. A. Mansoori, N. F. Carnahan, K. E. Starling, and T. W. Leland, Jr., J. Chem. Phys. **54**, 1523 (1971).
[13] L. Verlet and J. Weis, Phys. Rev. A **5**, 939 (1972).
[14] E. W. Grundke and D. Henderson, Mol. Phys. **24**, 269 (1972).
[15] G. Kahl and J. Hafner, J. Phys. F: Met. Phys. **15**, 1627 (1985).
[16] D. Saumon, G. Chabrier, and J. J. Weis, J. Chem. Phys. **90**, 7395 (1989).
[17] V. B. Warshavsky and X. Song, Phys. Rev. E **77**, 051106 (2008).
[18] C. Rascon, L. Mederos, and G. Navascues, Phys. Rev. E **54**, 1261 (1996).
[19] Y. Yu and J. Wu, J. Chem. Phys. **117**, 10156 (2002).
[20] H. Veith and E. Schroder, Z. Phys. Chem. Abt. A **179**, 16 (1937).
[21] P. van't Zeldfe, M. H. Omar, H. G. M. le Pair-Schroten, and Z. Dokoupil, Physica (Amsterdam) **38**, 241 (1968).
[22] X. Cottin and P. A. Monson, J. Chem. Phys. **105**, 10022 (1996).
[23] M. R. Hitchcock and C. K. Hall, J. Chem. Phys. **110**, 11433 (1999).
[24] H. S. Kang, C. S. Lee, T. Ree, and F. H. Ree, J. Chem. Phys. **82**, 414 (1985).
[25] D. Henderson and J. A. Baker, Phys. Rev. A **1**, 1266 (1970).
[26] R. Evans, in *Fundamentals of Inhomogeneous Fluid*, Edited by D. Henderson (Wiley, New York, 1992).
[27] B. Groh and B. Mulder, Phys. Rev. E **61**, 3811 (2000).
[28] Y. Rosenfeld, M. Schmidt, H. Lowen, and P. Tarazona, Phys. Rev. E **55**, 4245 (1997).
[29] T. Boublik, J. Chem. Phys. **53**, 471 (1970).
[30] W. G. T. Kranendonk and D. Frenkel, Mol. Phys. **72**, 715 (1991).
[31] J. G. Kirkwood and F. P. Buff, J. Chem. Phys. **19**, 774 (1951).
[32] J. K. Percus, in *The Equilibrium Theory of Classical Fluids*, edited by H. L. Frisch and J. L. Lebowitz (Benjamin, New York, 1964), p. II33.
[33] W. G. T. Kranendonk and D. Frenkel, Mol. Phys. **72**, 679 (1991).
[34] W. G. Hoover and F. H. Ree, J. Chem. Phys. **49**, 3609 (1968).
[35] A. A. Clifford, P. Gray, and N. Platts, J. Chem. Soc., Faraday Trans. **173**, 381 (1977).
[36] D. A. Kofke, Mol. Phys. **78**, 1331 (1993); J. Chem. Phys. **98**, 4149 (1993).
[37] A. L. Galbraith and C. K. Hall, Fluid Phase Equilib. **262**, 1 (2007).
[38] I. Szalai and S. Dietrich, Mol. Phys. **103**, 2873 (2005).
[39] B. Groh and S. Dietrich, Phys. Rev. E **63**, 021203 (2001).
[40] V. B. Warshavsky and X. Song, Phys. Rev. Lett. (submitted).
[41] V. B. Warshavsky and X. Song, Phys. Rev. E **73**, 031110 (2006).